JACS
JOURNAL OF THE AMERICAN CHEMICAL SOCIETY

Article

pubs.acs.org/JACS

Observation of Multipeak Collision Behavior during the Electro-Oxidation of Single Ag Nanoparticles

Stephen M. Oja,[†] Donald A. Robinson,[‡] Nicholas J. Vitti,[‡] Martin A. Edwards,[‡] Yuwen Liu,[‡] Henry S. White,*[,‡] and Bo Zhang*[,†]

[†]Department of Chemistry, University of Washington, Seattle, Washington 98195, United States
[‡]Department of Chemistry, University of Utah, Salt Lake City, Utah 84112, United States

Supporting Information

ABSTRACT: The dynamic collision behavior of the electro-oxidation of single Ag nanoparticles is observed at Au microelectrodes using stochastic single-nanoparticle collision amperometry. Results show that an Ag nanoparticle collision/oxidation event typically consists of a series of 1 to ∼10 discrete "sub-events" over an ∼20 ms interval. Results also show that the Ag nanoparticles typically undergo only partial oxidation prior to diffusing away from the Au electrode into the bulk solution. Both behaviors are characterized and shown to exist under a variety of experimental conditions. These previously unreported behaviors suggest that nanoparticle collision and electro-dissolution is a highly dynamic process driven by fast particle−electrode interactions and nanoparticle diffusion.

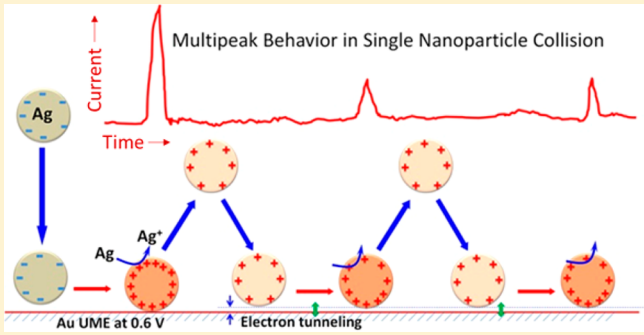

INTRODUCTION

Herein we report experimental observations of multipeak collision behavior during the electrochemical oxidation of single Ag nanoparticles (NPs). Our results indicate that the oxidation of these NPs occurs in several temporally resolved and discrete events, rather than one longer event as previously reported.

Stochastic single-NP collision amperometry is a method used to electrochemically detect single NPs that was first introduced by the Lemay group.[1] This initial report demonstrated a current inhibition when single NPs were adsorbed on an ultramicroelectrode surface and partially blocked the flux of redox-active molecules to the electrode. Depending on the relative size of the analyte particle and the recording electrode, this inhibition method can be used to detect a variety of analyte species, ranging from larger polymer spheres[1,2] and lipid vesicles[3] to smaller virus particles[4] and individual protein molecules.[5] In 2007, the Bard group published the method of electrocatalytic amplification (EA), which allows single catalytic NPs to be detected when they collide on a relatively inert electrode.[6] The EA detection scheme is a powerful analytical method and enables one to study electrocatalytic properties of NPs at a true single-particle level.[7] The literature published on this method has grown significantly since the initial report, as it has been applied in various schemes to detect a multitude of NPs under many different conditions.[8−13] Realizing the lack of chemical resolution as one of the limitations in amperometric recording, the Zhang group has used fast-scan cyclic voltammetry (FSCV) to obtain chemical resolution and determine electron-transfer kinetics in single-particle collisions.[14,15]

The Compton group adapted these ideas to the detection of NPs via the direct oxidation of the NPs themselves in a method they call anodic particle coulometry. In their initial report, this group reported the detection of single Ag NPs using a glassy carbon microelectrode.[16] When the microelectrode was held at oxidizing potentials, single oxidative spikes in the current signal were observed that were attributed to the direct electro-oxidation of colliding Ag NPs. Additionally, the charge associated with each collision event was reported to be in agreement with the charge expected based on the NP size, indicating complete oxidation of the NPs. This method has since been extended to the detection of Au,[17] Ni,[18] Mo,[19] and various transition metal dichalcogenide[20] NPs, as well as coupled with optical microscopy for additional detection information.[21]

Detecting single NPs by their faradaic reaction gives a direct measure of the interaction of single NPs with an electrode surface. This is in contrast to the electrocatalytic amplification method, which relies on a catalytic reaction of an added redox species occurring on a NP to mediate detection. The latter strategy can make signal interpretation more difficult, as this mediating reaction must be considered along with any dynamics of the NP interacting with the electrode.

Following the work of Compton and co-workers, our initial motivation in the current investigation was to use oxidative collisions of single Ag NPs as a method to generate a known

Received: September 4, 2016
Revised: October 25, 2016
Published: December 11, 2016

DOI: 10.1021/jacs.6b11143
J. Am. Chem. Soc. 2017, 139, 708−718

amount of charge in a closed bipolar electrochemical reaction.[22−24] Our initial experiments in the electro-oxidation of single Ag NPs on a Au microelectrode have revealed unexpected particle dynamic behavior not previously reported. Our experiment is carried out by placing a 12.7 μm diameter Au microelectrode in a dilute (~30 pM) aqueous solution of dispersed citrate-capped, spherical Ag NPs (diameter 62 ± 13 nm). The solution also contains trisodium citrate to stabilize the NPs and KNO_3 to serve as an electrolyte that favors electrodissolution of the Ag NPs.[21] Under typical conditions, the detection solution contains 8 mM trisodium citrate and 20 mM KNO_3. The microelectrode is held at a potential versus an Ag/AgCl wire quasi-reference electrode, and the current is recorded over time.

At potentials positive of 0.2 V, we observe sharp oxidative spikes in the current (Figure 1a), which we attribute to the

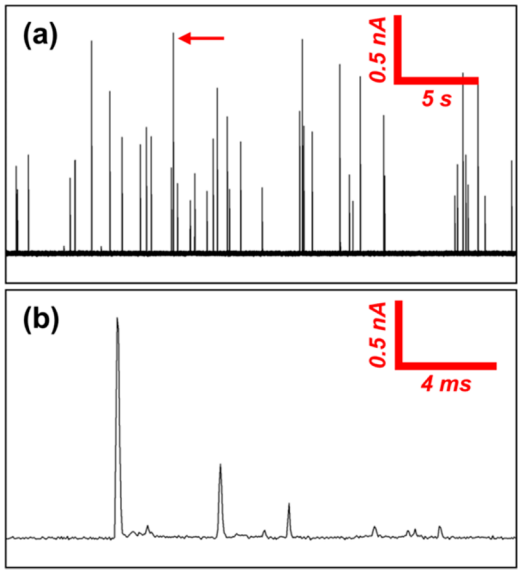

Figure 1. Example detection traces of Ag NPs colliding with an Au microelectrode poised at 0.6 V vs Ag/AgCl: (a) 30 s detection trace, with each spike corresponding to a particle colliding with the microelectrode and undergoing oxidation. (b) 20 ms zoom-in trace of the event in (a) indicated with the red arrow. As seen, each spike in (a) is made up of several smaller, discrete spikes. Further example traces are shown in section S3 of the Supporting Information. Conditions: 30 pM Ag NPs (60 nm diameter), 8 mM trisodium citrate, 20 mM potassium nitrate, and pH 7.7.

electro-oxidation of single Ag NPs colliding with the microelectrode in accordance with previous reports.[16,25] However, in contrast to the previous work on this topic, we have discovered that the electro-oxidation of single Ag NPs colliding with a Au detection microelectrode is a highly dynamic and complex electrochemical process: A single NP collision event contains several discrete fast subcollision events (Figure 1b). Our experiments show that "one" of these current spikes previously reported is really a series of smaller, discrete spikes spaced apart by ~1 ms (Figure 1b). Moreover, we observe that the total charge passed during these events equates to partial oxidation of the NPs. These new and surprising results show that NP electro-oxidation can involve highly dynamic behavior that can only be observed at the single-NP level.

In this paper, we propose a model based on electrostatics and nanoparticle random walk to explain the experimental observations. Our model suggests that the multipeak collision behavior is caused by a single NP moving in and out of contact with the microelectrode surface during a collision event. The initial NP/electrode contact is driven by a strong electrostatic attraction resulting in a direct electrical contact and a large Ag oxidation signal. However, subsequent subcollision events are likely affected by a change in the electrostatic potential on the remaining NP; charge transfer at the NP/electrode contact is via electron tunneling resulting in smaller Ag oxidation signals compared to the initial subpeak. We propose that NP motion at the electrode/solution interface is primarily driven by Brownian motion and that there is a finite probability of losing the NP into the bulk solution leading to incomplete NP dissolution. This mechanism is supported by preliminary lattice random walk simulations of particle diffusion and collision/reaction that closely match the experimental chronoamperometric results. Our findings reveal that NP interactions at an electrode surface are highly dynamic, a result broadly relevant to many current studies focused on the electrochemical detection and study of single NPs.

EXPERIMENTAL SECTION

Chemicals and Nanoparticle Detection Solution. Silver nitrate, trisodium citrate, citric acid, ferrocenedimethanol, and potassium nitrate were all used as received from Sigma-Aldrich. Deionized water (>18 MΩ·cm) was obtained through a Barnstead Nanopure water purification system and used for all aqueous solutions.

The Ag NPs used in experiments conducted at the University of Washington were prepared in-house by citrate reduction.[26] All glassware used in the synthesis was cleaned with aqua regia prior to use. First, 100 mL of aqueous 1 mM $AgNO_3$ was brought to a boil. While stirring, 2 mL of 1% (w/w) trisodium citrate was added. The reaction solution first turned yellow and then gray-orange after a few minutes. This solution was stirred and refluxed for 1 h, after which point it was cooled to room temperature. The solution was then centrifuged at 8000 rpm for 20 min, and the resulting supernatant was removed. The precipitate was redispersed in 100 mL of fresh aqueous 10 mM trisodium citrate solution and sonicated for 5 min. This centrifugation cycle was repeated once, and the precipitate was again dispersed in 100 mL of 10 mM trisodium citrate, which was used as the stock NP solution for all experiments.

Ag NPs were imaged and sized by transmission electron microscopy (TEM, Figure S1). The Ag NPs were drop-cast onto a carbon-coated Formvar copper TEM grid (Ted Pella) and imaged with an FEI Technai G2 F20 TEM operating at 200 kV. NP sizes were measured using ImageJ software.[27] The histogram of the NP size distribution and corresponding Gaussian fit were created using Origin software (OriginLab Corporation). The particles were approximately spherical with an average diameter of 62 ± 13 nm. Using this average diameter and the amount of Ag ions used in the synthesis, an upper limit for the particle concentration in the stock solution was calculated as 9.1×10^{10} particles/mL (or 150 pM). This concentration assumes that all Ag ions were reduced into NPs and that no NPs were lost in the centrifugation steps. The typical NP detection solution was prepared by combining the stock NP solution, 100 mM KNO_3, and 10 mM trisodium citrate in a 1:1:3 ratio by volume, resulting in an approximate NP concentration of 30 pM. This solution has a pH of 7.7 and was found to give stable NP detection over a period of tens of minutes. The solutions used for NP detection experiments at different electrolyte concentrations and pH values are described in the following sections and in the Supporting Information.

All data reported in the main text employed the above Ag NPs unless explicitly noted. Independent Ag NP collision experiments were also performed at the University of Utah using NPs commercially sourced from nanoComposix, Inc. (stock solution: 910 pM Ag NPs in 2 mM sodium citrate buffer, pH 7.5, and the average diameter was 71 ± 8 nm). Results and solution compositions using the commercially

DOI: 10.1021/jacs.6b11143
J. Am. Chem. Soc. 2017, 139, 708−718

supplied Ag NPs are identified whenever presented as "University of Utah Ag NPs". The results using both in-house synthesized 62 ± 13 NPs (University of Washington) and the commercial 71 ± 8 nm NPs (University of Utah) gave qualitatively similar and consistent results.

Electrochemical Measurements. The single-NP amperometry experiments at the University of Washington were carried out using an Axopatch 200B integrating patch-clamp amplifier (Molecular Devices) interfaced to a PC through a Digidata 1440A digitizer (Molecular Devices). The Axopatch was used in V-clamp mode with whole cell β = 1 and the low-pass filter set to 1 kHz. The single-nanoparticle detection experiment with potential pulsing (for data presented in Figure 5 of the main text) was carried out using a Chem-Clamp potentiostat (Dagan Corporation) in place of the Axopatch 200B. A headstage of N = 0.01 and 1 kHz low-pass Bessel filter were used with the potentiostat. The potential pulses were generated with an in-house LabView (National Instruments) program. Amperometric traces were recorded using pClamp 10.4 Axoscope software (Molecular Devices) with a 50 kHz sampling rate. Current spikes were analyzed and integrated using pClamp 10.4 Clampfit software (Molecular Devices), and histograms of the events with corresponding Gaussian fits were created using Origin software. The amperometry experiments at the University of Utah were carried out using a Pine bipotentiostat (Model AFRDE5) integrated with Chem-Clamp voltammeter/amperometer (Dagan Corporation) with a 3-pole low-pass Bessel filter operating at 10 kHz, unless otherwise noted. Data were acquired using a PC-6251 card from National Instruments and recorded with LabView. Current spikes were analyzed and manually integrated with OriginPro 9.1.

All experiments were performed using a two-electrode setup placed in a lab-built Faraday cage. A 12.7 μm diameter Au disk electrode was used as the working electrode in all experiments conducted at the University of Washington. This electrode was fabricated by sealing a 12.7 μm diameter Au microwire (Alfa-Aesar) in a borosilicate capillary (Sutter Instrument Co.) and making connection to the Au with tungsten wire and Ag paint (Dupont) through the back end of the capillary. Experiments at the University of Utah were performed with a 12.5 μm diameter Au electrode purchased from CH instruments. The Au electrodes were cleaned via mechanical polishing in 0.05 μm alumina slurry and rinsed thoroughly before each detection experiment. Experiments performed at the University of Utah included an electrochemical cleaning step whereby the potential was cycled from −0.8 to 1.2 V vs sat. $Hg/HgSO_4$ reference electrode at 100 mV/s in 0.1 M $HClO_4$ until a reproducible voltammogram was obtained, typically no more than 10 cycles. A Ag/AgCl wire was used as the counter and quasi-reference electrode (QRE) in all Ag NP collision experiments.

All potentials are reported as V vs Ag/AgCl QRE, which was calibrated to the standard hydrogen electrode (SHE) by comparing the half-wave potential ($E_{1/2}$) of ferrocenedimethanol determined by cyclic voltammetry using Ag/AgCl QRE with the $E_{1/2}$ vs $Hg/HgSO_4$ (sat. K_2SO_4, CH Instruments) reference electrode. The ferrocenedimethanol $E_{1/2}$ was determined to be −0.15 V vs $Hg/HgSO_4$ and −0.01 V vs Ag/AgCl QRE. Because the $Hg/HgSO_4$ reference electrode is 0.64 V vs SHE, the Ag/AgCl QRE was then calibrated to a potential of ~0.50 V vs SHE.

RESULTS AND DISCUSSION

Observation of Multipeak Collision Behavior at Different Potentials. Figure 1a shows an example 30 s amperometric trace of Ag NP detection where the gold microelectrode was held at a potential of 0.6 V vs Ag/AgCl. About 40 large oxidative spikes can be seen on top of a stable baseline current. The frequency of these oxidative spikes is ~1.3 Hz and is in reasonable agreement with the theoretical maximum collision frequency of 3.2 Hz, which can be calculated based on the size and concentration of the NPs and the radius of the probe electrode (see page S3 of the Supporting Information for details).[28] The higher predicted collision frequency may be due to an overestimated particle concentration and the fact that the "sticking" probability was considered as 100% in the calculation. One can estimate that the sticking probability of Ag NPs at the electrode surface is roughly 41% based on the measured collision frequency and the prediction. Three key features can be seen in this experiment. First, the anodic detection of Ag NP collision is extremely straightforward and highly reproducible. Second, the detection is stable over a long period of time. Although only a 30 s trace is shown in Figure 1a, this detection can last for more than 2 h without noticeable changes to the baseline current, the noise level, or the frequency and amplitude of detection events. Third, a significant variability is observed in the current amplitude of the detected events, which range from 400 to 1500 pA. The variation probably reflects differences in the NP−electrode contact and nanoscale heterogeneity on the surface of the Au electrode or particle-to-particle variability.

One of the most striking results is the discovery of multiple anodic current subpeaks in nearly every single detection event. We noticed that upon expanding the time axis of a detection event each event consists of several discrete oxidative current spikes. Figure 1b shows an example of this multipeak collision behavior, where an oxidation event consists of >1 "sub-peak," which is observed in ~90% of all detection events; rare examples where only one oxidation peak was observed occurred at high overpotentials (≥0.6 V) and are shown in section S11 of the Supporting Information. Figure S2 shows multiple examples of Ag NP oxidation events at four different potentials: 0.3, 0.4, 0.5, and 0.6 V. A quick examination of all the detection events reveals some interesting trends. First, nearly all of the detection events end within 20 ms. The probability of observing a second particle colliding the same electrode, when the averaging collision frequency is 1.3 Hz, can be easily estimated using the Poisson distribution to be ~2.5%. This indicates that the chance of observing a second particle hitting the same electrode within the 20 ms duration is quite low and that each subpeak observed in a NP detection event is caused by the same particle interacting with the electrode. Second, the number of subpeaks in each detection event is somewhat random, ranging from 1 subpeak for <10% of the total events to as many as 15 subpeaks for some of the more complex events. Third, the current magnitude of the first subpeak is generally the largest among all the subpeaks, while the magnitudes of the subsequent subpeaks are also quite random in each detection event. Fourth, some of the subpeaks last only a fraction of a millisecond indicating a very fast transient contact with the electrode surface. Moreover, the peak−peak spacing between neighboring subpeaks is on the order of 1 ms. These important features have been summarized in greater details in the following section and in Figure 2. This remarkable NP collision behavior, which indicates that the oxidation of single Ag NPs on an Au microelectrode typically occurs in 1 to ~10 discrete events, has only been briefly mentioned as a possibility in a recent report but has not been explicitly discussed in the literature.[29]

This interesting multipeak collision behavior begs the question of why an Ag NP is typically oxidized in several small, discrete events rather than a single large one. To better understand this behavior, we carefully analyzed the subpeaks present in Ag NP oxidation events recorded at four different detection potentials. Figure 2 shows the results of the analysis for the first six subpeaks of an event. We chose 6 subpeaks because most of the detection events contain less than 6 subpeaks in the detection period. The mean area, height, and duration of each subpeak are plotted in Figures 2a−c,

DOI: 10.1021/jacs.6b11143
J. Am. Chem. Soc. 2017, 139, 708−718

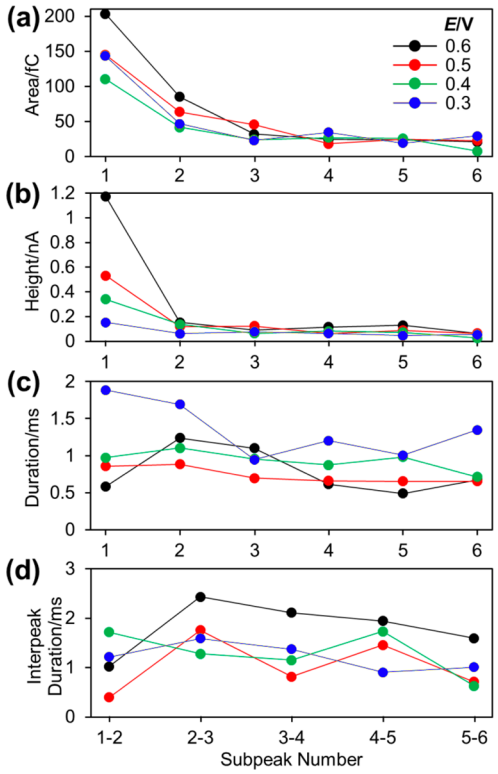

Figure 2. Analysis of the first six subpeaks for 25 random oxidation events recorded at each of four different detection potentials. (a–c) Mean subpeak area, height, and duration, respectively. (d) Mean duration between subpeaks. Conditions: 30 pM Ag NPs (60 nm diameter), 8 mM trisodium citrate, 20 mM potassium nitrate, and pH 7.7.

respectively, and the mean duration between subpeaks is plotted in Figure 2d. In terms of the number of subpeaks present per event, both the mean and median number were 4–5 subpeaks per event at all four detection potentials.

This detailed analysis confirms our above qualitative description of the overall trends. The first subpeak typically has the largest area and peak height. The peak area progressively decreases with subsequent subpeaks and levels out after the fourth subpeak. The peak height sharply decreases after the first subpeak and is roughly constant for subsequent subpeaks. The height of the first subpeak shows a very clear potential dependence, with a higher detection potential yielding a greater height. This increasing trend is likely due to an increasing overpotential driving the electro-oxidation at a greater rate. It is interesting to note that very high maximum current densities are observed (calculated as the peak height/NP surface area), with the first subpeak at a potential of 0.6 V yielding a density of nearly 10 A/cm^2. This high current density is a result of a higher overpotential, the fast radial type diffusion at a spherical NP electrode, and the high availability of Ag atoms at the pure metal NP surface. The typical duration of each subpeak is roughly 1 ms, as is the typical duration between each subpeak.

The total charge obtained from the integration of an entire single Ag NP oxidation event quantifies the total amount of Ag oxidized per NP collision event and can be used to calculate the apparent particle size. NP diameters were calculated as shown in previous reports (see page S6 of the Supporting Information for details). Figure 3 shows a plot of the size distribution of the

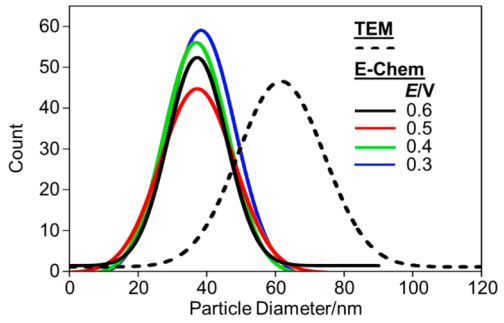

Figure 3. Comparison of Ag NP diameters as measured by TEM imaging (see section S1 of the Supporting Information for details) and single-NP electrochemical detection, assuming the charge measured corresponds to oxidation as explained in detail in section S4 of the Supporting Information.

NPs as determined by TEM imaging (dashed black line) and as calculated from the charge measured by single-NP detection at 4 different potentials (solid lines). As seen, the particle size measured by TEM (62 nm) is significantly larger than the particle size determined from electrochemical detection (~37 nm). This indicates incomplete oxidation of the Ag NPs upon collision with the electrode. In fact, the diameters reported here suggest that only about 25% of an Ag NP is oxidized during collision.

This result is remarkably different from previous reports using this method, which found the electrochemical measurement of Ag NPs to agree well with their known size.[16,17] Although we do not know exactly the origin of this discrepancy, we do note two major differences in our experimental setup that provide some explanation. First, the electrode material used in this work is Au, whereas all the work from the Compton group was performed on glassy carbon or carbon fiber electrodes. Second, the acquisition settings used in this work are also drastically different from the previous work. Despite the fact that the majority of the previous works on this topic do not comment on the data acquisition settings (filter frequency, sampling rate), we uncovered two Ag NP collision papers[30,31] that do report the use of 100 and 250 Hz low-pass Bessel filters. In contrast, data in our work were filtered at 1 kHz, except in the Supporting Information where the filter frequency was systematically varied to explore filtering effects on the response. The effect of different filter choices is shown in Figure S8. Using experimental conditions that yielded multipeak behavior when data were acquired at 1 and 10 kHz, we show that a 100 Hz filter renders multipeak behavior invisible; instead, multiple peaks are observed as peak with longer duration. The exact reason to the discrepancy in completeness in NP oxidation is still unclear as the filter settings do not change the total charge collected during a collision; see Figure S8 and Table S2.

Dependence on the Electrolyte Concentration. We found that both the multipeak behavior and partial oxidation behavior persisted under a variety of detection conditions as described below and in the Supporting Information. First, we altered the concentration of the supporting electrolyte KNO_3 from 0 to 25 mM (in the presence of 10 mM trisodium citrate). The use of supporting electrolyte in an electrochemical measurement helps to rapidly establish a potential drop at the electrode/solution interface in addition to minimizing the solution resistance and the *iR* drop. In this experiment, the presence of supporting electrolyte is expected to promote Ag

DOI: 10.1021/jacs.6b11143
J. Am. Chem. Soc. 2017, 139, 708–718

oxidation and dissolution. However, one should also note that the use of excess salt is prohibited because it decreases the stability of the colloidal solution causing NPs to aggregate. Ag NP detection at different concentrations of KNO_3 was carried out as follows. We started with a solution of 4:1 by volume 10 mM trisodium citrate:Ag NP solution. Since the Ag NP solution also contained 10 mM trisodium citrate, this gave an initial concentration of 10 mM trisodium citrate. Particle detection was carried for about 10 min at a detection potential of 0.6 V vs Ag/AgCl using this solution. The KNO_3 concentration was then increased by adding an aliquot of a solution that was 100 mM KNO_3 and 10 mM trisodium citrate, along with an appropriate aliquot of Ag NP solution to ensure that both the trisodium citrate concentration and Ag NP concentration remained constant. Particle detection was then carried out using this new solution for about 10 min. Sequential increases in KNO_3 concentration were continued in this fashion.

Figure S4 shows the current−time traces of three representative NP oxidation events at each of five different KNO_3 concentrations. As can be seen, the multipeak behavior persists at all concentrations of KNO_3. Table 1 gives a summary of the detection data at different KNO_3 concentrations. One can clearly see an increasing trend in the frequency of detection as the electrolyte concentration was increased from 0 to ∼20 mM. However, the detection frequency decreases as the KNO_3 concentration was further increased, suggesting that the NP stability may be negatively affected in the presence of excess electrolyte. The initial increase in detection can be understood from the increasing driving force for Ag oxidation with increasing electrolyte concentration, which increases the probability that a NP collision event will produce an observable oxidation current. This result clearly demonstrates the importance of carefully controlling the salt concentration in NP collision experiments.

Table 1. Statistics for Ag NP Collisions at Different Concentrations of KNO_3[a]

[KNO_3] (mM)	n	f (Hz)	Q (fC)	Std Dev (fC)
0	18	0.03	117	77
3.8	23	0.04	214	236
7.3	12	0.02	206	167
10.4	49	0.08	215	164
13.3	79	0.13	182	156
16	136	0.23	201	131
18.5	383	0.65	194	101
20.7	402	0.69	203	105
22.9	234	0.38	174	81
24.8	215	0.36	140	76

[a]Here, n is the number of oxidation events recorded in a 10 min recording, and f is the frequency of the oxidation events. Q and Std Dev were determined by a Gaussian fit of a histogram of the events. Q is the estimated mean value of the charge passed during an oxidation event as determined by the center of the Gaussian fit, and Std Dev is the standard deviation associated with Q. For KNO_3 concentrations of 0, 3.8, and 7.3 mM, there were not enough data points to perform an accurate Gaussian fit. Therefore, the Q and Std Dev values reported for these concentrations were calculated straight from the data rather than the Gaussian fit.

Dependence on the Citrate Concentration. In order to further understand the role of citrate ions in the detection and electrodissolution of Ag NPs, we also altered the concentration of trisodium citrate in the solution from 10 to 26 mM. Ag NP detection was carried out in the same manner as the above KNO_3 concentration experiment. We started with a solution of 4:1 by volume 10 mM trisodium citrate:Ag nanoparticle solution, giving an initial concentration of 10 mM trisodium citrate. At no point was any KNO_3 added to the detection solution in this experiment. Particle detection was carried for about 10 min at a detection potential of 0.6 V vs Ag/AgCl using this solution. The trisodium concentration was then increased by adding an aliquot of a solution that was 100 mM trisodium citrate, along with an appropriate aliquot of Ag nanoparticle solution to ensure that the Ag nanoparticle concentration remained constant. Particle detection was then carried out using this new solution for about 10 min. Sequential increases in trisodium citrate concentration were continued in this fashion.

Table 2 gives a summary of the detection data at different trisodium citrate concentrations, and Figure S5 shows the current−time traces of three representative NP oxidation events at four different trisodium citrate concentrations. Once again, while the frequency of detection changed, multipeak detection and partial NP oxidation were observed at all trisodium citrate concentrations. The citrate ions are used in the initial synthesis process of Ag NPs, and their presence help stabilize the NPs from aggregation. These citrate ions likely form a ligand layer around the Ag NP surfaces adding to their negative surface charges. As such, the initial increase in the detection could be partially due to the added stability of NPs and some additional electrostatic effects between negatively charged Ag NPs and the positive probe electrode. The extremely low detection frequency at the highest citrate concentration could possibly be due to stronger shielding effects from extra citrate molecules in the ligand shell. Alternatively, the Ag colloid most likely becomes unstable at higher ionic strength, causing a rapid decrease in the overall particle concentration and diffusion rate, thus lowering the observed collision frequency at the Au electrode.

Table 2. Statistics for Ag NP Collisions at Different Concentrations of Trisodium Citrate (Na_3Citrate)[a]

[Na_3 citrate] (mM)	n	f (Hz)	Q (fC)	Std Dev (fC)
10	5	0.008	170	171
13.4	33	0.05	524	492
16.5	314	0.53	227	177
19.4	545	0.93	155	132
22.0	331	0.56	117	72
26.2	60	0.08	88	77

[a]For trisodium citrate concentrations of 10 and 13.4 mM, there were not enough data points to perform an accurate Gaussian fit. Therefore, the Q and Std Dev values reported for these concentrations were calculated straight from the data rather than the Gaussian fit. The Q and Std Dev values reported for the other concentrations were determined using the Gaussian fit.

Dependence on the Solution pH. We also measured Ag nanoparticle collisions under four different pH conditions: 10.1, 7.7, 5.5, and 4.4. The motivation of this pH experiment is to rule out the possibility that the multipeak behavior involves the formation of an insulating layer of Ag oxide. Since our typical detection solution is slightly basic (pH ∼8), we hypothesized that the Ag NPs may be oxidized to form Ag oxide rather than Ag^+ ions. As such, running the same experiment in an acidic

DOI: 10.1021/jacs.6b11143
J. Am. Chem. Soc. 2017, 139, 708−718

environment would facilitate the dissolution of Ag oxide and reduce the probability of observing multipeak oxidation behavior. Figure 4 shows 20 ms long amperometry traces of

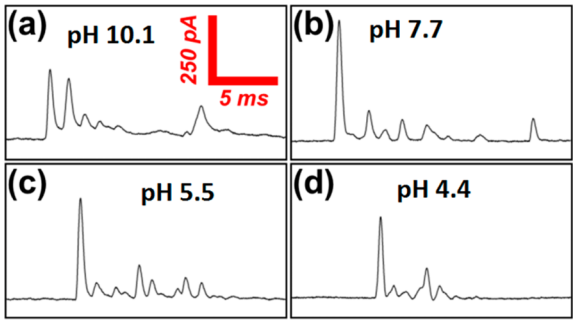

Figure 4. Amperometric traces (20 ms) showing a representative detection event at each of four pH values (labeled). As seen, similar multipeak behavior occurs under all four conditions. The detection potential was 0.6 V for all four solutions. See section S7 of the Supporting Information for a detailed analysis of the effect of pH on collisions.

representative detection events at the four different pH values. As can be seen, multipeak behavior again occurs under all four conditions. Analysis of the electrical charge of the detection events also indicates partial NP oxidation under all four pH values. These results further confirmed our prediction of the Ag^+ ions as the product species in the electro-oxidation of Ag NPs.

NP Collision in a Potential Pulse Experiment. We performed a further experiment designed to help determine the Ag^+ ions as the product resulting from the electro-oxidation of the Ag NPs. In these measurements, we performed an experiment in which the detection microelectrode was rapidly pulsed between a reducing (−0.2 V) and oxidizing (0.4 V) potential while measuring the current. The goal was to see if Ag^+ ions created during the oxidation of an Ag NP could be collected by electrochemical reduction. Figure 5a shows a 0.5 s section of a current−time trace for a pulsing frequency of 5 Hz. As can be seen, an occasional collision event is observed when the electrode is at an oxidizing potential (Figure 5b).

To analyze this data, we integrated the charge associated with each potential pulse and background-subtracted this value by the average charge of the 10 pulses before and after it. We then plotted these values as a scatter plot (Figures 5c), with one (x, y) data point representing the charges associated with the oxidation and subsequent reduction from a single potential pulse cycle. As seen in the scatter plots, the majority of the data points are clustered about the origin, indicating no above-average charge detection. However, it is clear that there are several points with above-average oxidation charges, which indicate the detection of a collision event. This is also evident upon comparison with the control experiment without Ag NPs, as shown in Figure S6, in which all data points are clustered near the origin. In Figure 5c, which is the result of potential pulsing at 5 Hz, the data are centered about $y = 0$, indicating no product collection on the subsequent reduction pulse. However, in Figure 5d, which is the result of potential pulsing at 50 Hz, these points are centered on a negatively sloped line. This indicates product collection during the subsequent reduction pulses in an amount proportional to the amount oxidized. Since collection of the oxidation product only occurs at a high pulsing frequency, this suggests that the oxidation

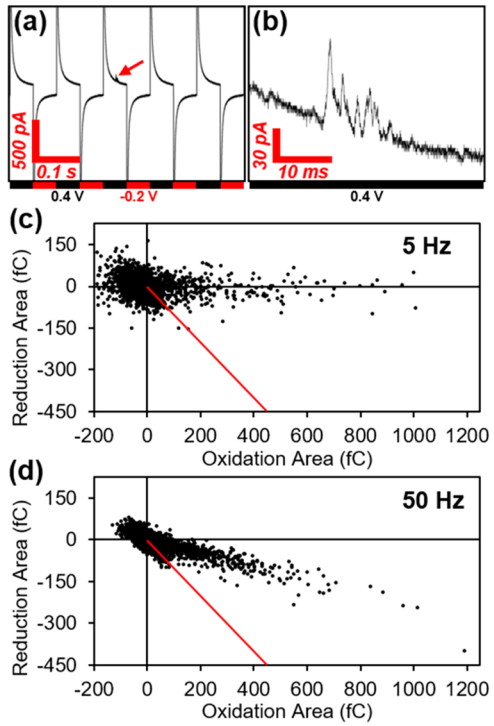

Figure 5. Results of an Ag NP detection experiment with potential pulsing. (a) Section of a current−time trace from a detection experiment with a pulsing frequency of 5 Hz. (b) Zoom-in of the collision event indicated in (a) with the red arrow. (c) and (d) Scatter plots of baseline subtracted charges from consecutive oxidation and reductions with pulsing frequencies of 5 and 50 Hz, respectively. Red lines represent $y = -x$. A solution of 30 pM NPs, 8 mM trisodium citrate, and 20 mM KNO_3 at pH 7.7 was used in this experiment. Control measurements with no NPs present in the solution are presented in section S8 of the Supporting Information.

product quickly diffuses away from the electrode upon oxidation, which we believe is consistent with the formation of Ag^+ ions as the electro-oxidation product.

Effect of Solution Viscosity. Our new hypothesis on the observation of multipeak behavior is that a single Ag NP undergoes repeated collision and electro-oxidative partial dissolution upon first contact with the electrode. The repeated collision is mainly driven by random Brownian motion in the vicinity of the electrode surface. Each contact can be considered as a subcollision event in which part of the NP is oxidized leading to a short subpeak observed in the entire detection event. The detection event comes to an end when the NP diffuses far into the bulk solution. The number of subcollision events is somewhat random because the motion of the particle is described by a random walk. In order to further support this hypothesis, we have conducted additional experiments to examine the dependence of multipeak behavior on solution viscosity.

Here, we used a glycerol/water mixture to increase the viscosity of the solution and study the effects of decreasing the diffusion coefficient of Ag NPs. Figure S7 shows the CVs of the 12.5 μm diameter Au electrode in ferrocenedimethanol in water and 25% w/w glycerol/water mixed solution. The diffusion limited current in aqueous solution is about 2 times larger than that in the glycerol/water mixture; hence, the viscosity of the glycerol/water mixture is ∼2 times higher at this ratio. Figure 6 shows representative current−time traces for individual Ag NP

DOI: 10.1021/jacs.6b11143
J. Am. Chem. Soc. 2017, 139, 708−718

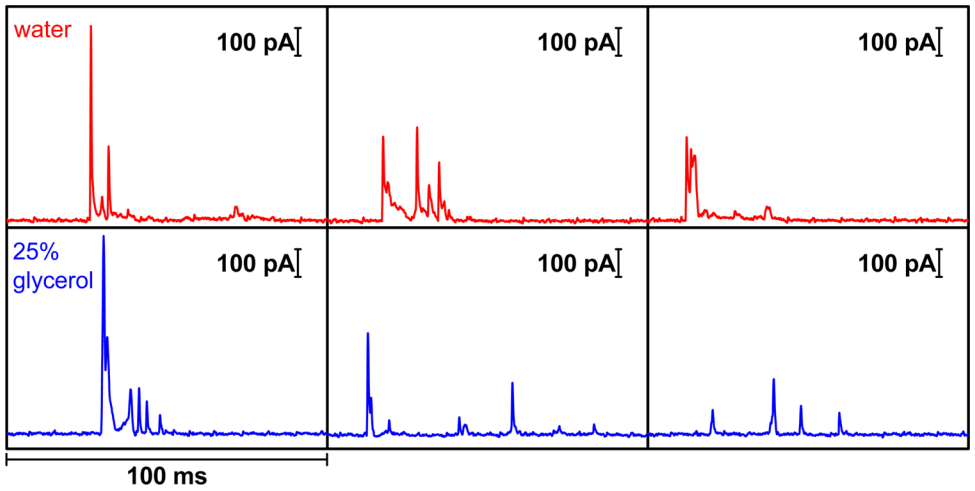

Figure 6. Current–time traces showing three representative Ag NP oxidation events in all-aqueous (red trace) and 25% w/w mixed glycerol/water solutions (blue trace). Solution contained 18 pM Ag NPs (70 nm, University of Utah NPs) in 6 mM trisodium citrate and 20 mM KNO_3, pH 7.

oxidations. As one can see, the partial oxidation subpeaks for the purely aqueous solution occur in a more rapid succession in comparison to the glycerol/water mixture due to the lower viscosity of the solution. The corresponding distributions of interpeak time intervals are shown in Figure 7, sampled from 26

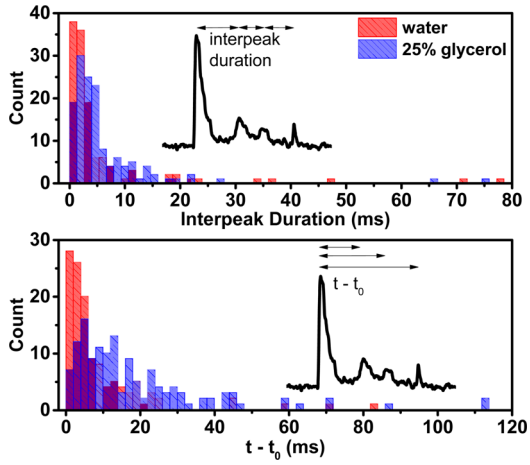

Figure 7. Histograms of time intervals in between subpeaks of Ag NP oxidation events for solutions in all-aqueous (red) and 25% w/w glycerol/water (blue). The *x*-axis in the top panel corresponds to the time intervals between each consecutive subpeak while that for the bottom panel is the time interval between each subpeak and the first subpeak of the collision event (t_0), as represented by the embedded example *i*–*t* traces. Solution contained 18 pM Ag NPs (70 nm, University of Utah NPs) in 6 mM trisodium citrate and 20 mM KNO_3, pH 7.

Ag NP impact events for water and 19 events in the glycerol–water mixture. The duration between consecutive subpeaks in 25% glycerol is longer on average (by a factor of ~2) than that obtained for water. The average time between any given subpeak and the initial primary peak is also noticeably longer on average, yet varied widely in the glycerol/water case. The presence of multiple oxidation peaks in each NP detection event and the extended interpeak time intervals in the 25% w/w glycerol/water suggest that repeated collision and diffusion of the remaining Ag NPs is important in the observation of multipeak oxidation behavior.

Our Proposed Mechanism for Multipeak Collision. Drawing on all of the results discussed, we hypothesize that the interesting multipeak oxidation behavior of single Ag NP collision events is due to diffusion of the Ag NP in and out of contact with the Au microelectrode. As faradaic oxidation of the Ag NP should only occur when the NP is within ~1 nm of the electrode surface, diffusional motion could repeatedly turn the Ag oxidation off and on, giving rise to multiple, closely spaced oxidation peaks. This explanation fits with much of the observed data here. The observation of multipeak behavior at different potentials, electrolyte concentrations, and pH values is consistent with this explanation, as none of these conditions should significantly change the diffusion of the NPs. Moreover, the prolonged interpeak durations of the multipeak behavior recorded in the glycerol/water mixed solution further supports our proposed mechanism. Lastly, the observation of incomplete NP oxidation and partial dissolution is consistent with this explanation, as the NP may only be in the ~1 nm vicinity of the electrode surface for a brief period of time before permanently diffusing away from the electrode surface. Therefore, only a portion of the NP may be oxidized during collision.

One of the most important questions in this NP collision experiment is what causes the particle to leave the electrode surface after its initial contact with the electrode and after each subsequent subcollision event. In addition, there are several other interesting characteristics in the multipeak current–time response. First, the initial subpeak is considerably higher than other subpeaks and is almost always the largest peak in current magnitude in the entire NP collision sequence. Furthermore, the remaining subpeaks are relatively uniform in peak height each measuring only ~15% of the initial subpeak, as revealed from Figure 1b. Second, the duration of all subpeaks stays relatively constant at around 1 ms at all voltages. Third, the average spacing between adjacent subpeaks is also relatively uniform at ~1 ms in aqueous solutions.

We propose the mechanism illustrated in Figure 8 to explain how the multipeak collision behavior observed with single Ag NPs. As shown in Figure 8, a freely diffusing Ag NP is negatively charged due to the use of citrate ions as surface ligands. The negative surface charges remain intact prior to its initial contact with the electrode in a collision event and are the primary driving force for a strong electrostatic interaction with an electrode resting at a positive potential, e.g., +0.6 V vs Ag/

DOI: 10.1021/jacs.6b11143
J. Am. Chem. Soc. 2017, 139, 708–718

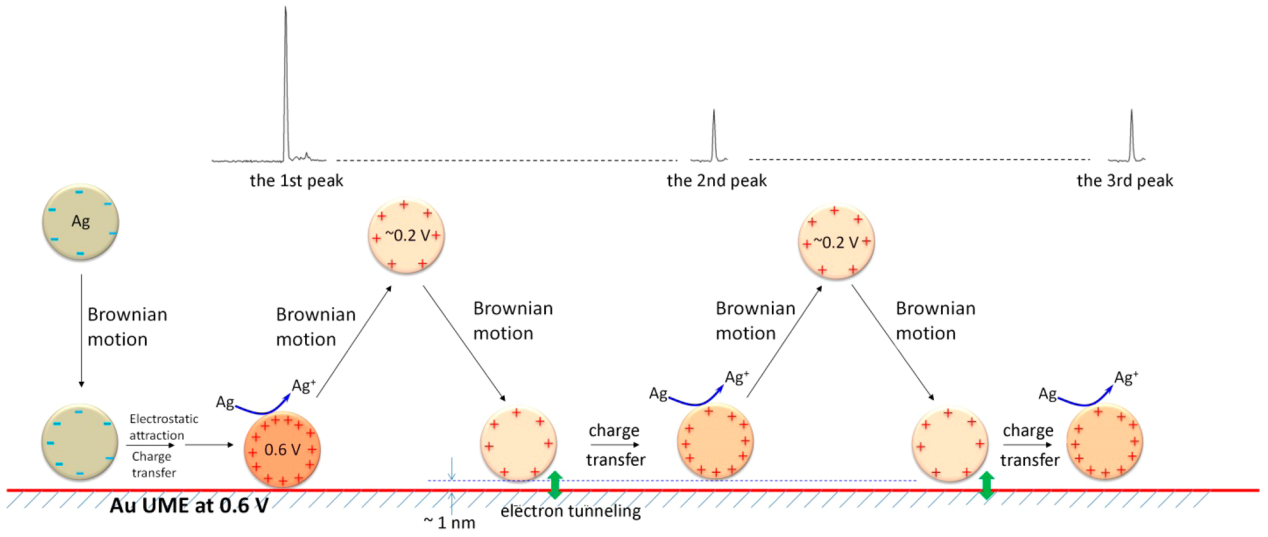

Figure 8. Proposed scheme for the observed multipeak collision behavior of single Ag NPs.

AgCl. Upon collision with electrode, however, one can expect that the NP will quickly adopt the same electrostatic potential as the recording electrode, which can have two immediate consequences: (1) The Ag atoms sitting at the NP surface will be oxidized leading to an increasing anodic current as the NP is quickly charged up. (2) The electrostatic interaction between the NP and the electrode will quickly change from strong attraction to strong repulsion as the electrostatic potential on the NP changes from negative to the same positive potential as on the electrode. This repulsive force drives the NP away from the electrode surface leading to a quick decrease in the Ag oxidation current.

Figure 8 also helps to address the key fact that the initial current spike has a larger magnitude than the remaining subpeaks. This is difficult to explain based on the particle size considering that there is only a minimal change in the size of the particle after each oxidation subevent. As our results indicate, on average only ~25% of a particle is oxidized in an entire collision event; this size decrease is likely only partially responsible for this behavior. We believe the smaller amplitude of subsequent subpeaks is mainly caused by a change in surface potential on the particle as compared to the initial surface potential prior to the collision event. The first hit in a collision always results in the largest current amplitude due to a strong electrostatic attraction between the positively charged electrode and the negatively charged particle, as shown in Figure 8. The NP is expected to establish a direct electrical contact with the electrode at the point of contact resulting in an Ag oxidation current that is only limited by the electron-transfer kinetics and the size of the NP. After the first hit, the NP becomes positively charged and leaves the electrode carrying the same electrostatic potential as the electrode, e.g., 0.6 V. At this time, however, the NP would not be electrochemically stable due to its high positive potential and must undergo further dissolution of Ag to Ag^+ to dissipate some of its positive charge until the electrostatic potential on the particle is no longer sufficient to drive further oxidation of Ag. Our results show the lowest potential required to oxidize Ag is around 0.2 V. As such, the expected surface potential on the remaining NP should be around 0.2 V after the first collision. Although ligand adsorption and rearrangement could occur and may slightly change the electrostatic potential, the remaining NP should still be positively charged before the second hit. This results in a repulsive NP−electrode interaction when the NP returns to the electrode surface by Brownian motion. It is reasonable to expect that the NP can only approach to the electrode to within a finite distance due to this repulsive interaction. As such, the current magnitude of Ag oxidation would be limited by the rate of electron tunneling at the point of the second subcollision in addition to being affected by the particle size and potential. In summary, the limited electron tunneling rate and its exponential decay with distance are responsible for the smaller current magnitude of the subsequent subpeaks. Figure 8 also illustrates a third subcollision event, which is quite similar to the second subcollision in both the mechanism and the current response. This process is expected to repeat until Brownian motion carries the NP back into the bulk solution or the NP is completely oxidized.

It is interesting to ask how many subpeaks one can collect out of an entire collision event and if an Ag NP can be entirely dissolved during the collision. As described previously, we believe the NP motion at the electrode surface is primarily driven by Brownian motion. Electrostatics may play a key role only when the particle approaches the electrode surface at very small distances, e.g., <5 nm, depending on the thickness of the electrical double layer. As such, the number of subpeaks and their spacing would be largely random and should be better understood by random walk simulation. On the one hand, it is quite possible that a small NP can be completely oxidized in one or two subcollisions resulting in full dissolution. On the other hand, for a larger particle, there is also a finite chance of a NP completely escaping from the electrode surface before completely dissolving. This explains that the NPs are only partially oxidized during collision in our experiments.

Lattice random walk simulations using the method previously reported by White and White,[32] modified to update the reduced Ag particle size upon collision with the electrode, support the conclusion that peaks in current arise from multiple collisions of a single particle with the electrode. A single adjustable parameter, the current density for Ag particle oxidation, was set to 1000 A cm^{-2}. A summary of results of these simulations is provided in Figures 9 and 10 (a full account of simulation details will be reported in an upcoming work).

DOI: 10.1021/jacs.6b11143
J. Am. Chem. Soc. 2017, 139, 708−718

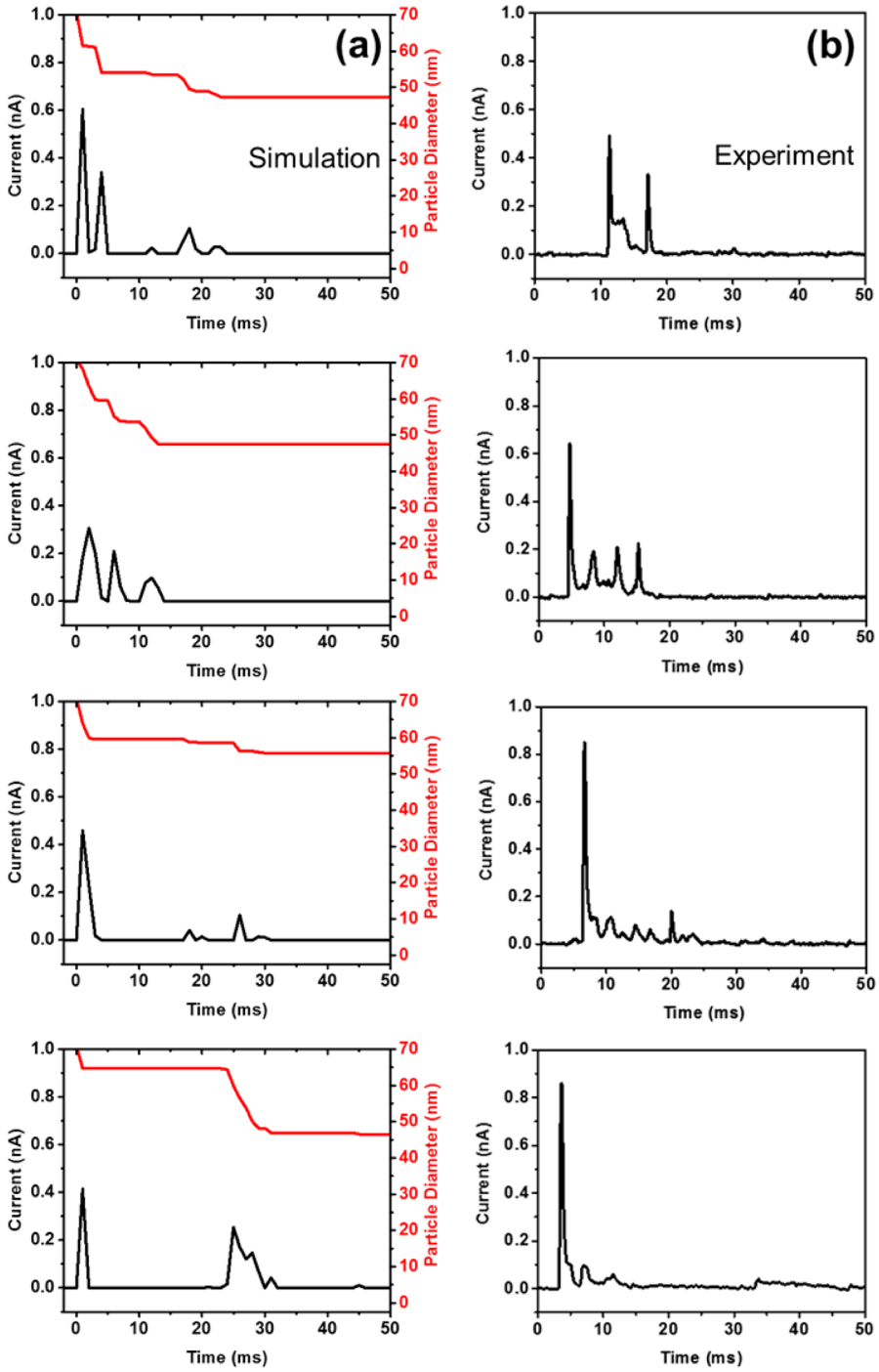

Figure 9. (a) Current−time traces (black) from random walk simulations of single 70 nm Ag NPs, where collision of the NP with a microelectrode causes oxidation and a change in the particle size. Shown in red is the corresponding NP diameter as a function of time. (b) Experimental amperometric traces for collisions of 70 nm citrate-stabilized Ag NPs (University of Utah NPs) acquired at 0.5 V. Solution contained 18 pM Ag NPs in 6 mM trisodium citrate and 20 mM KNO_3, pH 7.

Figure 9a shows four simulated amperometric example traces of the collision-dissolution process for a 70 nm Ag NP, which have been postfiltered at 1 kHz to allow direct comparison with representative experimental traces shown in Figure 9b. Due to the postsimulation filtering at 1 kHz, each simulated current subpeak event shown in Figure 9a corresponds to many elastic collisions with the electrode, on the order of hundreds of collisions per subpeak. Both simulated and experimental amperometric traces show multipeak behavior on a similar time scale, in addition to the previously noted experimental trend of decreasing subpeak currents with increasing time. The simulated nanoparticle radius as a function of time is included in Figure 9a (red curve), showing how the much the particle size decreases each time it collides with the electrode.

Our simulations also predict partial oxidation of the Ag nanoparticles prior to their diffusion away from the microdisk electrode, as can be seen in Figure 10, which compares histograms of integrated charge passed during a multipeak collision event for both experiments and simulations. In both cases, the average charge passed was 0.8 ± 0.4 pC, which

DOI: 10.1021/jacs.6b11143
J. Am. Chem. Soc. 2017, 139, 708−718

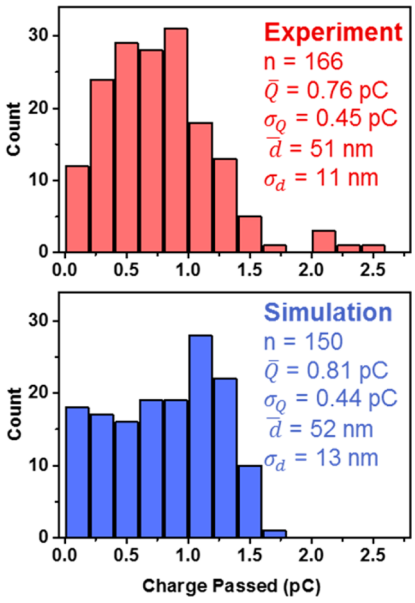

Figure 10. Histograms of the charge passed during the oxidation of individual 70 nm Ag NPs colliding with an electrode coming from experiments (top) and random walk simulations (bottom). Inset are the number of NPs analyzed/simulated (n), the average charge passed ($\bar{Q}$), its standard deviation (σ_Q), and the average NP diameter calculated according to eq S3($\bar{d}$) and its standard deviation (σ_d). Both data sets were filtered at 1 kHz. The charge was calculated by integration of current over a period of 50 ms after the first collision (current peak). Solution contained 18 pM Ag NPs in 6 mM trisodium citrate and 20 mM KNO_3, pH 7.

corresponds to oxidation of roughly 50% of a 70 nm Ag NP, resulting in a spherical diameter of ~50 nm after 50 ms. Such high level of agreement between the experimentally observed and simulated amperometric response further supports the stepwise electrodissolution model controlled by diffusion and multiple collisions at the Au electrode−solution interface. Full details of these simulations will be reported elsewhere.

CONCLUSIONS

We have revealed that the electro-oxidation of single Ag NPs colliding with a Au detection microelectrode is a highly dynamic process. Under our experimental conditions, a typical detection event is observed as a series of discrete oxidation subpeaks rather than one large peak. We have also revealed that the Ag NPs do not undergo complete oxidation. Both of these behaviors were shown to exist under a wide range of detection conditions. We have presented a model to explain these observations. Our model suggests that the electro-oxidation of a single citrate-stabilized Ag NP during a collision event is primarily driven by the potential on the electrode and the electrostatic effects at the electrode/NP interface. The initial NP/electrode contact is likely a direct electrical contact allowing free flow of electrons resulting in a large Ag oxidation signal. However, the electron-transfer process at the NP/electrode interface in subsequent subcollisions is likely driven by electron tunneling due to electrostatic repulsion and a finite distance established between the positively charged NP and the electrode. This results in smaller Ag oxidation signals compared to the initial subpeak. The NP motion at the electrode/solution interface is largely driven by Brownian motion that results in a finite probability of losing the NP back into the bulk solution and incomplete dissolution, as supported by random walk simulations. This study reveals that NP interactions with an electrode surface are highly dynamic, and it should be broadly relevant to many current studies focused on the electrochemical detection and study of single NPs.

ASSOCIATED CONTENT

Supporting Information

The Supporting Information is available free of charge on the ACS Publications website at DOI: 10.1021/jacs.6b11143.

TEM characterization, calculation of expected collision frequency, examples of events used for the subpeak analysis, calculation of nanoparticle size based on measured charge, more details on the detection experiments at different electrolyte concentrations and pH values, control experiment for NP detection with potential pulsing, and experiments using commercial Ag NPs: discussion of the effect of filtering frequency on the data, single peaks at high overpotentials, and potential dependence of detection data. (PDF)

AUTHOR INFORMATION

Corresponding Authors

*E-mail: white@chem.utah.edu.
*E-mail: zhang@chem.washington.edu.

ORCID

Henry S. White: 0000-0002-5053-0996
Bo Zhang: 0000-0002-1737-1241

Notes

The authors declare no competing financial interest.

ACKNOWLEDGMENTS

This research was supported by AFOSR MURI (FA9550-14-1-0003). Part of this work was conducted at the University of Washington NanoTech User Facility, a member of the National Science Foundation, National Nanotechnology Infrastructure Network (NNIN). Y.L. acknowledges a Fellowship from China Scholarship Council (201506275068).

REFERENCES

(1) Quinn, B. M.; van't Hof, P. G.; Lemay, S. G. *J. Am. Chem. Soc.* **2004**, *126*, 8360−8361.
(2) Fosdick, S. E.; Anderson, M. J.; Nettleton, E. G.; Crooks, R. M. *J. Am. Chem. Soc.* **2013**, *135*, 5994−5997.
(3) Lebègue, E.; Anderson, C. M.; Dick, J. E.; Webb, L. J.; Bard, A. J. *Langmuir* **2015**, *31*, 11734−11739.
(4) Dick, J. E.; Hilterbrand, A. T.; Strawsine, L. M.; Upton, J. W.; Bard, A. J. *Proc. Natl. Acad. Sci. U. S. A.* **2016**, *113*, 6403−6408.
(5) Dick, J. E.; Renault, C. R.; Bard, A. J. *J. Am. Chem. Soc.* **2015**, *137*, 8376−8379.
(6) Xiao, X.; Bard, A. J. *J. Am. Chem. Soc.* **2007**, *129*, 9610−9612.
(7) Xiao, X.; Fan, F. -R. F.; Zhou, J.; Bard, A. J. *J. Am. Chem. Soc.* **2008**, *130*, 16669−16677.
(8) Cheng, W.; Compton, R. G. *TrAC, Trends Anal. Chem.* **2014**, *58*, 79−89.
(9) Kwon, S. J.; Bard, A. J. *J. Am. Chem. Soc.* **2012**, *134*, 7102−7108.
(10) Alligrant, T. M.; Anderson, M. J.; Dasari, R.; Stevenson, K. J.; Crooks, R. M. *Langmuir* **2014**, *30*, 13462−13469.
(11) Alligrant, T. M.; Dasari, R.; Stevenson, K. J.; Crooks, R. M. *Langmuir* **2015**, *31*, 11724−11733.
(12) Kang, M.; Perry, D.; Kim, Y.-R.; Colburn, A. W.; Lazenby, R. A.; Unwin, P. R. *J. Am. Chem. Soc.* **2015**, *137*, 10902−10905.

(13) Dasari, R.; Robinson, D. A.; Stevenson, K. J. *J. Am. Chem. Soc.* **2013**, *135*, 570−573.
(14) Guo, Z.; Percival, S. J.; Zhang, B. *J. Am. Chem. Soc.* **2014**, *136*, 8879−8882.
(15) Percival, S. J.; Zhang, B. *J. Phys. Chem. C* **2016**, *120*, 20536−20546.
(16) Zhou, Y.-G.; Rees, N. V.; Compton, R. G. *Angew. Chem., Int. Ed.* **2011**, *50*, 4219−4221.
(17) Zhou, Y.-G.; Rees, N. V.; Pillay, J.; Tshikhudo, R.; Vilakazi, S.; Compton, R. G. *Chem. Commun.* **2012**, *48*, 224−226.
(18) Stuart, E. J. E.; Zhou, Y.-G.; Rees, N. V.; Compton, R. G. *RSC Adv.* **2012**, *2*, 6879−6884.
(19) Giovanni, M.; Ambrosi, A.; Sofer, Z.; Pumera, M. *Electrochem. Commun.* **2015**, *56*, 16−19.
(20) Lim, C. S.; Tan, S. M.; Sofer, Z.; Pumera, M. *ACS Nano* **2015**, *9*, 8474−8483.
(21) Brasiliense, V.; Patel, A. N.; Martinez-Marrades, A.; Shi, J.; Chen, Y.; Combellas, C.; Tessier, G.; Kanoufi, C. *J. Am. Chem. Soc.* **2016**, *138*, 3478−3483.
(22) Guerrette, J. P.; Oja, S. M.; Zhang, B. *Anal. Chem.* **2012**, *84*, 1609−1616.
(23) Cox, J. T.; Guerrette, J. P.; Zhang, B. *Anal. Chem.* **2012**, *84*, 8797−8804.
(24) Guerrette, J. P.; Percival, S. J.; Zhang, B. *J. Am. Chem. Soc.* **2013**, *135*, 855−861.
(25) Rees, N. V.; Zhou, Y.-G.; Compton, R. G. *ChemPhysChem* **2011**, *12*, 1645−1647.
(26) Turkevich, J.; Stevenson, P. C.; Hillier, J. *Discuss. Faraday Soc.* **1951**, *11*, 55−75.
(27) Schneider, C. A.; Rasband, W. S.; Eliceiri, K. W. *Nat. Methods* **2012**, *9*, 671−675.
(28) Kwon, S. J.; Zhou, H.; Fan, F. -R. F.; Vorobyev, V.; Zhang, B.; Bard, A. J. *Phys. Chem. Chem. Phys.* **2011**, *13*, 5394−5402.
(29) Kätelhön, E.; Tanner, E. E. L.; Batchelor-McAuley, C.; Compton, R. G. *Electrochim. Acta* **2016**, *199*, 297−304.
(30) Tanner, E. E. L.; Batchelor-McAuley, C.; Compton, R. G. *J. Phys. Chem. C* **2016**, *120*, 1959−1965.
(31) Batchelor-McAuley, C.; Ellison, J.; Tschulik, K.; Hurst, P. L.; Boldt, R.; Compton, R. G. *Analyst* **2015**, *140*, 5048−5054.
(32) White, R. J.; White, H. S. *Anal. Chem.* **2005**, *77*, 214A−220A.

DOI: 10.1021/jacs.6b11143
J. Am. Chem. Soc. 2017, 139, 708−718